ThC1-2

Inductance Compensation of Multiple Capacitors with Application to Common- and Differential-Mode Filters

Brandon J. Pierquet[†], Timothy C. Neugebauer[‡], and David J. Perreault[†]

[†]Laboratory for Electromagnetic and Electronic Systems
Massachusetts Institute of Technology, Cambridge, MA
[‡]Charles Stark Draper Laboratory, Cambridge, MA

Abstract— **Capacitor parasitic inductance often limits the high-frequency performance of Electromagnetic Interference (EMI) filters in both common- and differential-mode filtering domains. However, these limitations can be overcome through the use of specially-coupled magnetic windings that effectively nullify the capacitor parasitic inductance. This document explores the use of a single coupled magnetic winding to provide inductance compensation for multiple capacitors (e.g. both differential- and common-mode capacitors) simultaneously, reducing the number of coils previously required. The substantial advantages of this method are illustrated both in a proof-of-concept test circuit and in an improved version of an existing EMI filter. The coupling between multiple inductance compensation windings in a single filter enclosure is also investigated.**

I. INTRODUCTION

Electromagnetic interference (EMI) filters are an important part of many types of electrical equipment, and they play a critical role in meeting requirements for device compatibility. The size and performance of these filters are often limited by their component parasitics, such as the equivalent series inductance of capacitors and the equivalent parallel capacitance of inductors [1]–[12]. These limitations have generated recent interest in methods for compensating parasitics to increase filter performance [5]–[12]. For example, as shown in [5]–[7], coupled magnetic windings can be used to cancel the effects of capacitor parasitic inductance. Inductance cancellation windings can be used to reduce the filter volume and cost and/or increase its attenuation performance.

Conventionally, inductance cancellation windings have only been used with a single capacitor. In a filter designed for both common- and differential-mode filtering, this requires a number of windings to be used to compensate all capacitors. The simple EMI filter in Fig. 1 contains three capacitors: two line-to-common, and one line-to-line.

The goal of this document is to introduce the use of a single coupled magnetic winding to compensate for the effects of the parasitic inductance of two discrete capacitors, thereby saving precious space and added cost. Section II outlines the motivation for applying this concept to EMI filters, and demonstrates its application in experimental test cases. Section III follows with an application of the method to improve

an existing EMI filter. Section IV provides an analytic basis for the observed performance improvements, and Section V concludes the paper.

II. MULTIPLE ELEMENT INDUCTANCE COMPENSATION

A. Motivation

To understand why the use of a single magnetic winding to compensate for parasitics of two capacitors is of particular value in EMI filtering, consider the structure and operation of an EMI filter. Fig. 1 shows the basic structure of an EMI filter designed to attenuate both common-mode and differential-mode signals, along with representative source and load networks for performance evaluation. This circuit can be analyzed by separating its common-mode and differential-mode responses and treating these equivalent circuits as if they were independent [2]. The common- and differential-mode equivalent circuits are shown in Fig. 2.
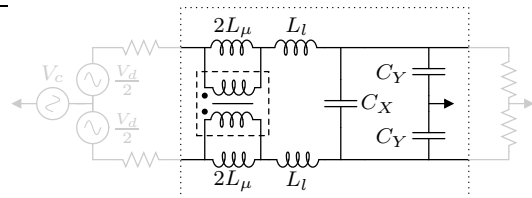

Fig. 1. Simple EMI filter circuit shown with representative source and load networks for performance evaluation. Some parasitic elements (such as capacitor equivalent series inductance) are not shown explicitly.

Now, if the circuit of Fig. 1 is augmented with inductance cancellation coils for each capacitor, the circuit in Fig. 4 is generated. In this new figure, the differential capacitor C_X is fitted with two inductance cancellation coils instead of only one to preserve circuit symmetry. Past work [5] has shown this to be as effective as a single coil, and Fig. 3 shows a photograph of this where the inductance cancellation windings are fabricated on a PCB.

It is desirable to implement the cancellation windings in a balanced fashion to avoid inserting an unbalanced circuit element within the otherwise well-balanced system. Without
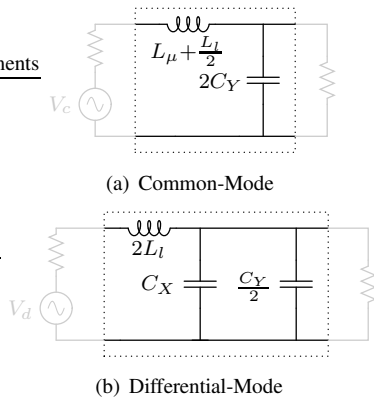
(a) Common-Mode

(b) Differential-Mode

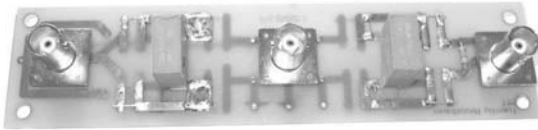Fig. 2. Models for the simple EMI Filter circuit of Fig. 1, decomposed into common- and differential-mode portions.

(a) Common-Mode

(b) Differential-Mode

Fig. 5. Simple EMI Filter circuit with balanced inductance cancellation of each capacitor, decomposed into common- and differential-modes.

Fig. 3. Test circuit with balanced inductance cancellation windings implemented in the printed circuit board. Performance of this filter has been previously shown [5].

winding to provide appropriate inductance compensation for two capacitors.

B. Implementation

To show experimentally that the use of a single inductance cancellation coil for two capacitors is feasible, a simple test filter was created with a planar winding mounted with EMI filter capacitors inside a shielded enclosure. Fig. 6 shows the filter along with the two Panasonic ECK-ATS472ME6 4700pF Y2 class ceramic capacitors used. This test filter does not directly examine common- and differential-mode testing, however it does provide a straightforward example how a single coil can support the compensation of inductance for two capacitors. A dimensioned line-art drawing of the coil, which was cut using an OMAX abrasive-jet cutter from a single piece of 1mm thick copper, is shown in Fig. 7. Based on simulation results from FastHenry [13], the coil itself has a maximum series inductance of 393.0nH, and a maximum equivalent shunt-path inductance of -63.2nH when used for single element inductance cancellation (in the magnetic winding T model). It should be noted that this coil was intentionally designed to be far over-sized for the amount of cancellation required; this was to allow for maximum flexibility in testing.

balancing the series inductances on both sides of the capacitor, a cross coupling between the differential and common-mode signal sources would result. By avoiding this coupling, the common- and differential-mode circuit equivalents remain straightforward, as illustrated in Figs. 5(a) and 5(b).
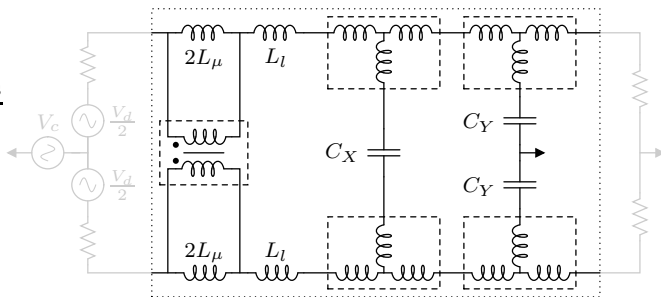

Fig. 4. Simple EMI Filter circuit from Fig. 1 with balanced inductance cancellation of each capacitor.

As shown in Fig. 4, the construction of an EMI filter with full, balanced inductance cancellation would require four magnetically coupled windings when constructed using the previously established method. These windings occupy additional space within the filter, and if placed in close proximity may exhibit secondary effects from magnetic coupling, complicating the design. The effects of coupling are investigated more thoroughly in Section II-C. Given these limitations, it would be a considerable improvement if the number of required windings could be reduced by utilizing a single
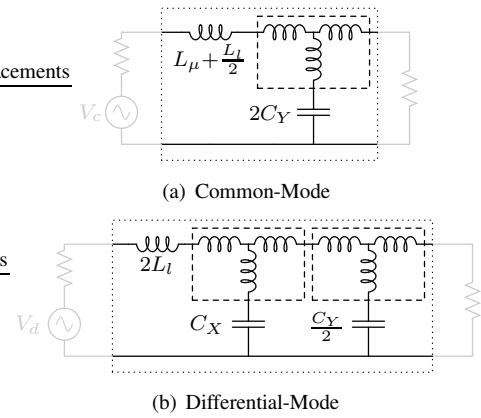
The procedure outlined here was developed for tuning the filter response of the two capacitors, and is one way a high performance filter response can be determined. Initially, the connection of capacitor C_1 is tuned to optimally cancel its parasitic inductance. This can be done by adjusting the connection point of the capacitor on the winding while observing the filter attenuation (e.g. with a network analyzer), and/or using methods associated with previously described techniques in [6]. Once its optimal position is found, the position of the capacitor is fixed. Following this, the connection of capacitor C_2 is tuned (with capacitor C_1 in place) to find an optimal filter response. This gives one possible combination of capacitor locations on the coupled winding that results in a high performance filter characteristic.

Experimental results for this test system are shown in Fig. 8, with data taken from an Agilent 4395A network analyzer
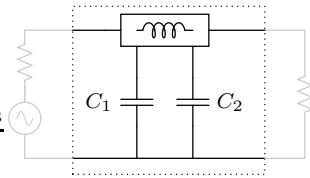
(a) Schematic
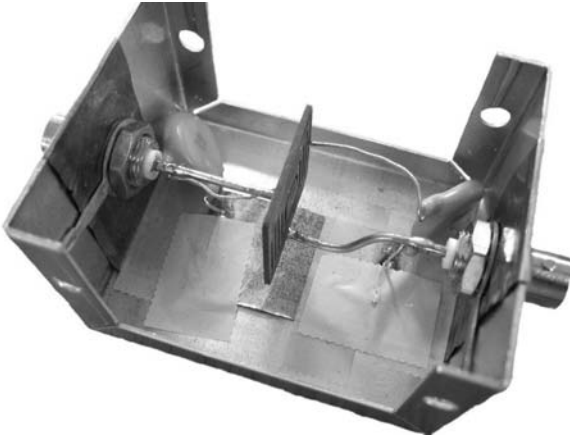
(b) Physical Layout

Fig. 6. Test filter for inductance compensation of two Panasonic ECK-ATS472ME6 4700pF ceramic capacitors using a single magnetic winding.
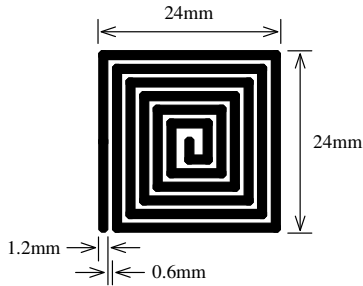

Fig. 7. Illustration of the planar winding used in the test filters of Section II, fabricated from 1mm thick copper. The total series-path inductance based on simulation is 393.0nH, and the maximum equivalent shunt-path inductance for a single element is -63.2nH (in the magnetic winding T model).

which provides 50Ω source and load impedances. Insertion gain measurements were made in accordance with those used to evaluate inductance cancellation performance in [5], [6] to allow for direct performance comparison. When tuning the response with only C_1, two measurements were taken for comparison: one with the capacitor connected directly at the input (source-side) terminal providing no cancellation, and one where the capacitor was connected to the cancellation coil at a location where the output response was optimal. The same approach was taken when tuning the response for the combination of C_1 and C_2: C_2 was connected either directly at the filter output (load-side) terminal or at a position optimizing the filter response with both capacitors.

The characterization results of the filter attenuation performance clearly show a dramatic improvement (as much as 35dB at high frequency) from the case where no compensation is
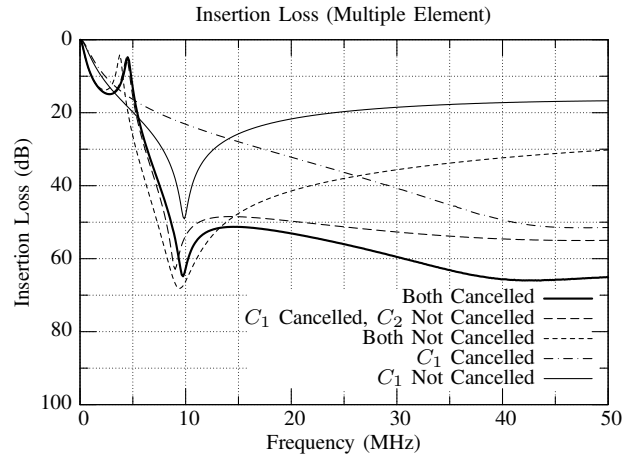

Fig. 8. Measured results from the test filter in Fig. 6 showing the performance of multiple-element inductance compensation.

provided (*Both Not Cancelled*) to the case where inductance compensation is provided for both capacitors (*Both Cancelled*). These results demonstrate that a single coupled magnetic winding can be used to provide inductance compensation for two capacitors, with dramatic performance improvement at high frequencies.

C. Coupling of Multiple Windings

When physically placing multiple magnetic windings in close proximity, linked magnetic flux between the windings can affect the predicted performance in various ways [8]. Thus, the implementation of multiple cancellation windings in a single filter may affect the inductance cancellation and filter performance. Here the effects of mutual coupling are explored when two coils are used to provide balanced inductance cancellation for both common- and differential-mode capacitors.
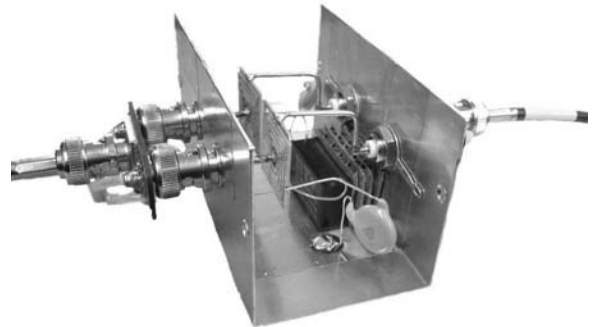

Fig. 9. Filter for investigation of common- and differential-mode coupling between inductance compensation windings.

Two additional filters (using the same windings shown in Fig. 7) were created to test two coil configurations having different magnetic coupling directions. In addition to a pair of line-to-ground (Y) capacitors (Panasonic ECK-ATS472ME6)

for common-mode filtering, these test filters incorporate a Rubycon 250MMCA334KUV class X2 line-to-line capacitor for differential-mode filtering. Fig. 9 is a photo of one of the filters, and shows its internal layout. Figs. 10 and 11 show the filter configurations and illustrate the difference between the two winding orientations.

Windings placed in the *same direction* each throw flux in a way which opposes the flux of its paired winding for common-mode currents, reducing each winding's effective inductance. In the case of the windings oriented in the *opposite direction*, the flux from each winding is reinforced by the other for common-mode currents, providing a coupling direction like that of a common-mode choke, and increasing each winding's effective inductance.
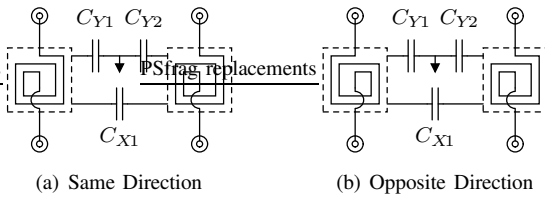

(a) Same Direction   (b) Opposite Direction

Fig. 10. Two orientations of coupled inductance compensation coils. The coils are of the type shown in Fig. 7. C_{Y1} and C_{Y2} are Panasonic ECK-ATS472ME6, C_{X1} is a Rubycon 250MMCA334KUV. The two circuits only differ with respect to mutual coupling among the coils.
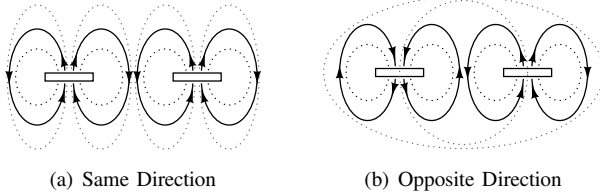

(a) Same Direction   (b) Opposite Direction

Fig. 11. Flux patterns for common-mode operation of the two magnetic winding configurations of Fig. 10. Windings oriented in the *same direction* generate flux in a way which opposes the flux of the paired winding for common-mode currents. Windings oriented in the *opposite direction* generate fluxes which reinforce each other, providing a coupling direction like that of a common-mode choke.

The tuning procedure used here is similar to the one used in the two-capacitor case in Section II-B. Initially, the connections of capacitors C_{Y1} and C_{Y2} are tuned simultaneously in the common-mode case to compensate for their parasitic inductances (while retaining a balanced configuration). Once the optimal positions are found, the positions of the capacitors are fixed. Following this, the capacitor C_{X1} is tuned in the differential-mode case by moving its connections on both coils symmetrically to find an optimal output response. Tuning is carried out in this order because ideally the addition of the differential-mode capacitor does not affect the common-mode response, while the reverse would not necessarily be true.

The experimental setup for calibration and measurement of the common- and differential-mode filter performances are taken from [14], with signal generation and measurement performed by the same Agilent 4395A Network Analyzer

as in Section II-B, with Mini-Circuits 180° power splitters (models ZSCJ-2-1 and ZSCJ-2-2) for dividing its output into differential signals, and custom-made common-mode splitters.
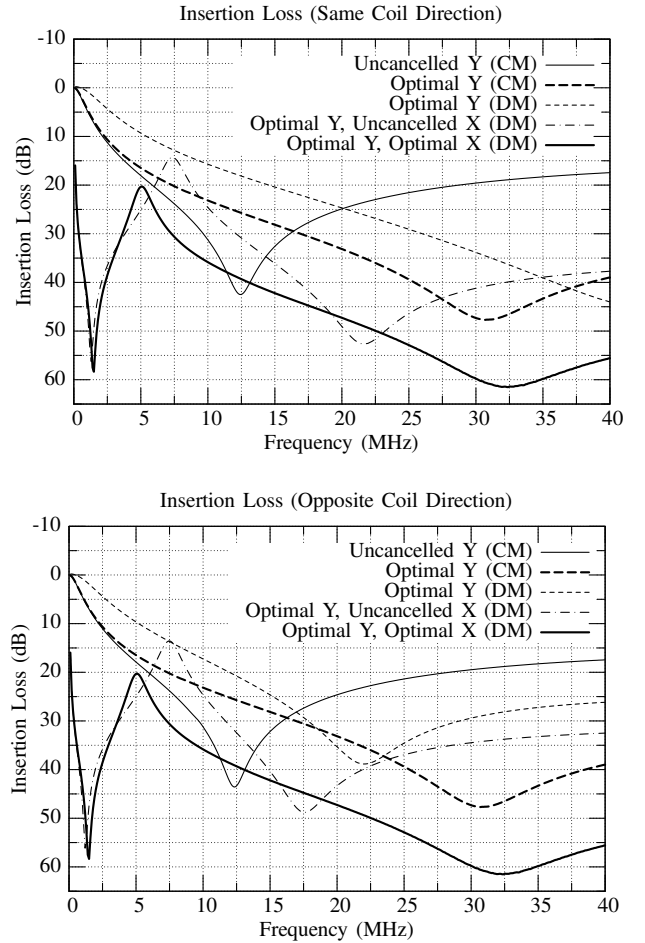

Fig. 12. Measured results from the coupled inductance compensation winding orientations of Fig 10, including both common-mode (CM) and differential-mode (DM) measurements.

In both winding configurations the target frequency for optimization was 30MHz, with measurements shown up to 40MHz. The two orientations possess similar optimized filtration performance, seen in the thicker traces of Fig. 12. The thinner traces in show additional measurements from intermediate steps in the tuning process.

The results show that in both winding orientations an equivalent inductance compensation improvement can be achieved for both the common- and differential-modes. This allows the orientation of the windings to be selected based on other factors (e.g. based on magnetic coupling with more dominant circuit parasitics). While the winding orientation does not influence the final optimized response in these filters, how each winding orientation achieves this optimum is slightly different. In Fig. 13 the connection locations for the filter capacitors are shown, corresponding to the optimal common- and differential-mode filter response from Fig. 12.

Due to the coupling in the common-mode, the connection
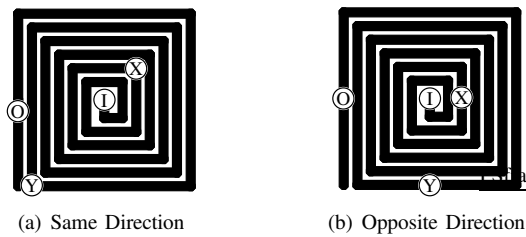
(a) Same Direction

(b) Opposite Direction

Fig. 13. Connection locations of capacitors corresponding to the results in Fig. 12. Only one winding of each pair is shown, the connections made to the other winding are symmetric. X represents the connection location of C_{X1}, Y represents the corresponding C_{Yn} connection location for that winding, I is connected to the input of the filter, and O represents the connection to the filter output.

for the C_{Yn} capacitor was closer to an end terminal on the winding in the *opposite direction* orientation than in the *same direction* orientation. Effectively, in the common-mode, the *opposite direction* orientation has a marginally higher inductance-per-turn than the *same direction* orientation, and thus requires a slightly reduced number of turns to achieve the same performance.

Even with the the windings in close proximity, the effects of magnetic coupling on the inductance compensation are minimal. In more extreme cases where the coupling is significantly higher, the observed effects may become more pronounced. Even in this case, however, an equivalent performance should be achievable given properly sized windings.

III. APPLICATION TO COMMERCIAL EMI FILTER

Having shown in the previous section that a single inductance cancellation winding can be used with two capacitors to improve filtration performance, and that the coupling orientation of multiple windings in a single filter does not adversely affect potential inductance compensation, the use of multiple element inductance compensation in the context of common- and differential-mode EMI filter is examined. A commercially-available filter is used as a starting point.

Figs. 14(a) and 14(b) show the schematic and physical views of the filter, which is rated for up to 250 volts and 25 amps of 50/60Hz alternating current. The large (15μH) series inductors L_{11} and L_{12} are particularly bulky, heavy, and expensive components of the commercial filter, and it would be desirable to eliminate them provided that filter performance is preserved. The series inductors were removed to provide working space for installing the inductance cancellation windings, and to provide an opportunity to offset their removal through use of the much smaller cancellation windings. Figs. 15(a) and 15(b) show the modified schematic and physical layout of the filter with the inductance cancellation windings installed. Additionally, Fig. 16 shows the folded design of the inductance cancellation coil used in this filter. As with the previous coil in Fig. 7, Fig 16 was cut with an abrasive-jet cutter, using 2mm thick copper for enhanced current carrying capacity. The flat winding structure is folded at the center of its longest side to form a square one-piece two-layer winding

with Mylar tape used as insulation between the layers. Based on simulation results, the coil is estimated to have a series inductance of 288.3nH, and a maximum equivalent shunt-path inductance of -81.2nH when used for single element inductance cancellation (in the magnetic winding T model). As in the previous test filters, the coil is purposefully over-designed for the required inductance cancellation to allow for additional design flexibility and testing.
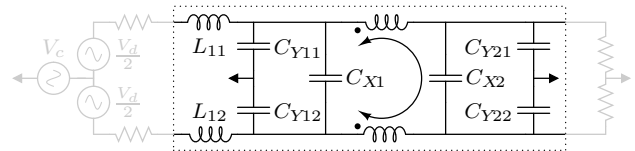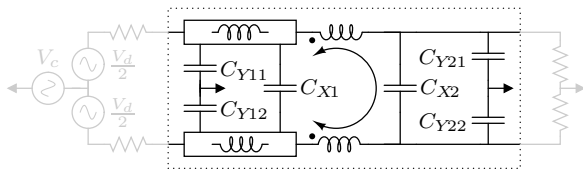

(a) Schematic
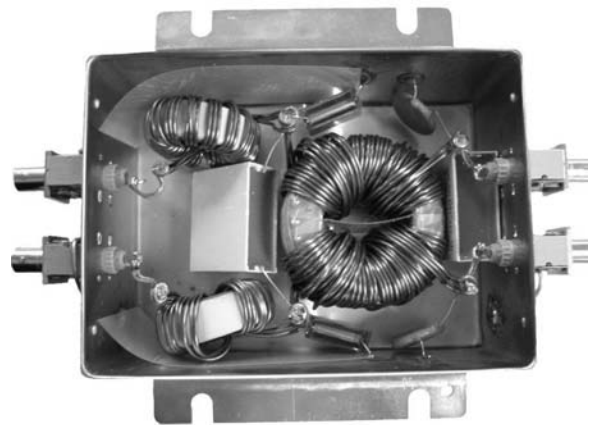
(b) Physical Layout

Fig. 14. Original Commercial EMI Filter. L_{11}, L_{12} are 15μH wound toroidal inductors, C_{Y11} and C_{Y12} are Rifa PME-271 47nF film capacitors, C_{X1} and C_{X2} are Vishay Roederstein F1772-522-2030 2.2μF film capacitors, C_{Y21} and C_{Y22} are 15nF ceramic capacitors, and the common-mode choke has a measured leakage inductances of 30.2μH and a magnetizing inductance of 4.45mH.

Common- and differential-mode measurements were taken of the unmodified filter, as well as an intermediate step before the inductance cancellation windings were installed. In this intermediate step, the large inductors L_{11} and L_{12} were removed and straight, solid 14ga wire was installed in their place. This configuration, referred to here as *Without Series Inductor*, was used as a baseline comparison for improvements based on inductance cancellation.

The tuning procedure outlined here is the same as the one used in Section II-C, and was developed for tuning the filter response due to the common- and differential-mode capacitors. Initially, the connections of common-mode capacitors C_{Y1} and C_{Y2} are tuned simultaneously to compensate (in a symmetric fashion) for their parasitic inductances. Once the optimal positions are found, the capacitors are permanently attached to their respective windings. Following this, the differential-mode capacitor C_{X1} is tuned by moving its connections on both coils symmetrically to find an optimal output response.

This order of tuning makes sense: the common- and differential-mode capacitors do not impact system perfor-

(a) Schematic
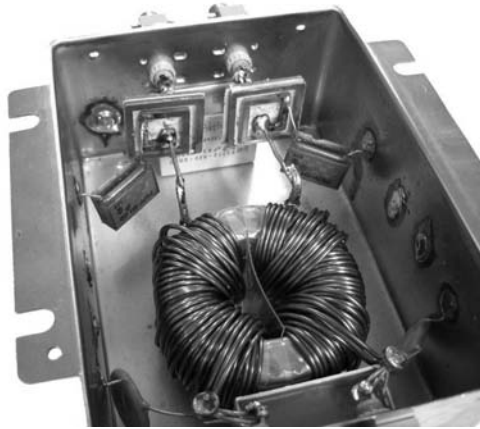
(b) Physical Layout

Fig. 15. Modified version of the EMI filter in Fig. 14 with L_{11} and L_{12} removed, and two inductance compensation windings installed.
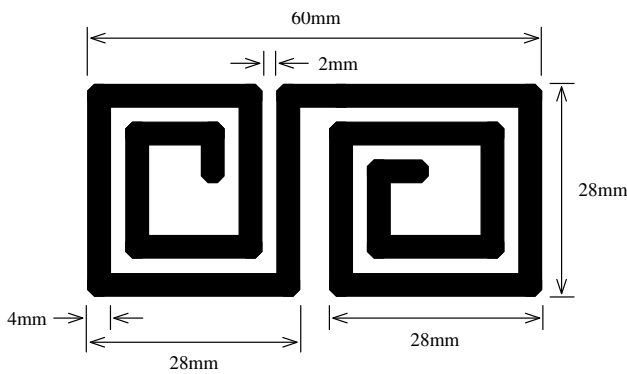

Fig. 16. Illustration of folded winding used for inductance compensation in the EMI filter of Section III, fabricated from 2mm thick copper. When folded, the total series inductance is 288.3nH, and the maximum equivalent shunt-path inductance for a single element is -81.2nH (in the magnetic winding T model).

mance in the same way. In Fig. 5(a) it can be seen that the common-mode equivalent circuit is not influenced by the differential-mode capacitance (or the inductance cancellation, other than through the fixed series inductance introduced by the winding); the common-mode filtration operates as if the differential-mode capacitor were an open circuit. However, the differential-mode filtration is dependent on the common-mode capacitance and inductance cancellation. This means that if the inductance compensation for the common-mode capacitance is optimized first, the inductance compensation for the differential-mode capacitor can be tuned subsequently without influencing the common-mode performance.

The results of the completed tuning are shown in Fig. 17

along with the stock and baseline filter configurations. It should be noted that tuning of both the common- and differential-modes is based on compromises between high and low frequency performance. This particular "optimal" output response chosen here may not be the highest achievable performance for a particular range of frequencies of interest.
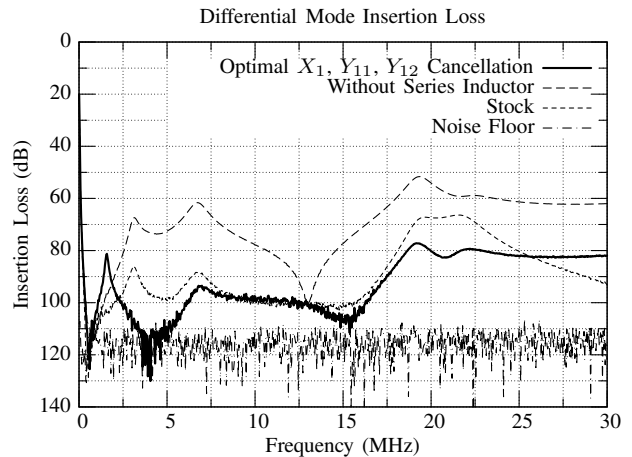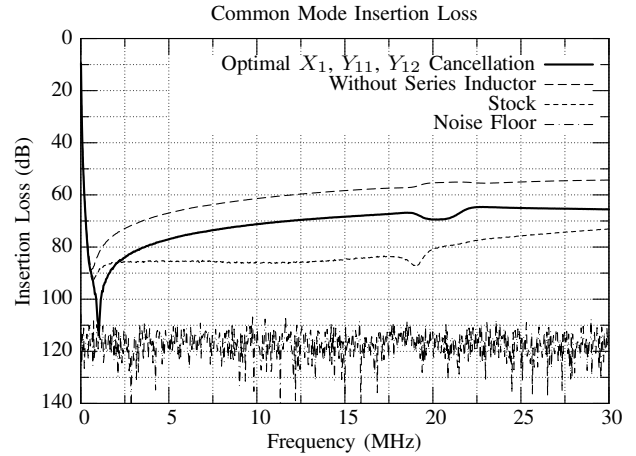

Fig. 17. Performance comparison of the commercially-available EMI filter in Fig. 14 and the modified version in Fig. 15, showing performance both without and with inductance compensation.

The results of incorporating the inductance cancellation coils reveal a dramatic improvement in the filtration performance for both the common- and differential-mode responses over the baseline (stock filter with L_{11} and L_{12} removed, labeled as *without series inductor*). The common-mode shows improvement across its full range, and the differential-mode shows substantial improvement over its full range except for the small resonance around 2MHz. (This small resonance is caused in part by the capacitor-inductor-capacitor π-section formed with the two capacitors attached to the inductance compensation winding in the differential-mode, and can be reduced by fabricating a winding with lower series inductance than the over-sized one used here.)

The common-mode performance with inductance compensation is somewhat worse ($\sim$10dB) than that of the stock filter

(with large inductors L_{11} and L_{12}), while the differential-mode performance is comparable. More importantly, the performance with the inductance cancellation windings exceeded the commercially-published performance specification of the stock filter (not shown), without requiring the large, expensive series inductors of the stock filter.

The results from this commercial EMI filter, as well as those from the test filters in Section II, show clearly that a single magnetically coupled winding can provide effective inductance compensation for two capacitors. Moreover, it is demonstrated that the performance of a commercial filter design can be preserved at lower component weight and cost through use of the proposed approach. It is anticipated that further substantial design improvements could be achieved in a filter expressly designed to take advantage of the inductance compensation method proposed here.

IV. Analytic Formulations

In this section an analytical basis is sought for the proposed method of compensating for the inductance of two capacitors using a single coupled magnetic winding. It is derived from an extension of the methods used to analyze single-capacitor inductance cancellation techniques. The predictions of this method are then compared to measured results to illustrate its usability.

A. Extended Cantilever Model

Analysis of inductance cancellation windings with a single capacitor is relatively straightforward since a two-port transformer model of the windings is used, which has only three independent terms. The number of independent terms needed to completely describe coupled magnetics with n terminals is given by $n(n+1)/2$ [15], which grows as the square of n.

Adding to the complexity is the fact that many models for multiple winding transformers either do not adequately model the complete transformer behavior, or have poor correlation and numeric conditioning to attempted measurements of model parameters from terminal characteristics [16], [17]. One model that is effective, and well conditioned for experimental parameter extraction, is the Extended Cantilever Model [15], [16].

The Extended Cantilever Model of a coupled system yields an equivalent circuit with directly measurable parameters and provides a direct mapping between circuit parameters and the inductance matrix parameters. It is also well conditioned numerically when dealing with small leakage fluxes or high coupling factors. The extended cantilever circuit model for a three-port system is shown in Fig. 18(a), with circuit parameters related to impedance matrix parameters as follows:

$$Z = sL \tag{1}$$

$$B = \begin{bmatrix} Z_{11} Z_{12} Z_{13} \\ Z_{21} Z_{22} Z_{23} \\ Z_{31} Z_{32} Z_{33} \end{bmatrix}^{-1} \tag{2}$$

$$N_k = \frac{Z_{1k}}{Z_{11}} \tag{3}$$

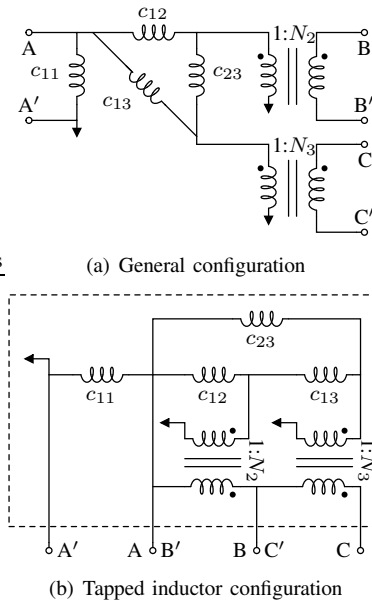(a) General configuration

(b) Tapped inductor configuration

Fig. 18.   Three-port extended cantilever models.

$$c_{11} = Z_{11} \tag{4}$$

$$c_{ij} = -\frac{1}{N_i N_j b_{ij}} \tag{5}$$

where b_{ij} is the $(i,j)^{\text{th}}$ element of B.

It should be clarified that the notation used to indicate the impedance matrix Z is representative of only the reactive component of Z due to the equivalent inductance; the extended cantilever model in [15] is formulated only with consideration to inductances. An extension which allows for full Laplace domain circuit elements can be found in [18], [19], however in the idealized case considered here, parasitic resistances and capacitances are assumed to be negligible.

B. Three-Port Analysis

Fig. 18(b) shows the application of the extended cantilever model to a center-tapped winding with two tap points. Fig. 19 shows additional circuit connections used for finding the system transfer function. The full transfer function for the system is given in Appendix I, and truncated versions are utilized in this section where appropriate.

By analogy to the case of inductance cancellation for a single capacitor, we desire to find conditions that drive the transfer function from the input source to the output voltage to zero (or close to zero). In finding where the transfer function goes to zero, conditions must be found where both the numerator becomes zero, and the denominator remains finite and non-zero. Starting from the numerator of the full transfer function in (10) from Appendix I, setting it equal to zero, refactoring, and dividing by the non-zero value of z_l, a condition is found in which a zero in the numerator can be generated:
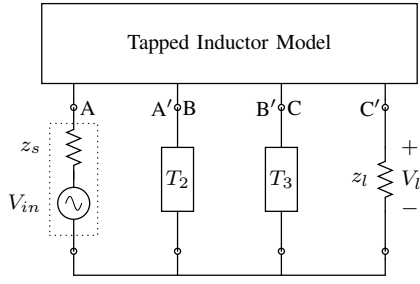
Fig. 19. Shared-terminal three-port circuit for use with the Extended Cantilever Model tapped-inductor configuration of Fig. 18(b). T_2 and T_3 represent the (inductive) high frequency impedances of the capacitors.

$$0 = Z_{13} \left(Z_{12} + Z_{23} + Z_{13} + Z_{22} \right) \\ - \left(T_2 - Z_{12} - Z_{13} \right) \left(T_3 - Z_{13} - Z_{23} \right) \qquad (6)$$

This result, considered by itself, provides a number of terms that can be adjusted to satisfy the equality. However, in the case of common-mode and differential-mode filtering there are additional constraints that must be considered.

C. Common- and Differential-Mode Optimization

As described previously in Sections II-C and III, in an EMI filter the common- and differential-mode capacitors do not impact system performance in the same way: the common-mode filtration operates as if the differential-mode capacitor were an open circuit, while the differential-mode filtration is dependent on the common-mode capacitance and its inductance cancellation. To find the optimal cancellation for the common-mode capacitor, the transfer function in (10) is considered at the limit where $T_3 \rightarrow \infty$ (the differential-mode capacitance is a virtual open circuit for common-mode signals).

$$H(s) = \frac{\left(T_2 - Z_{13} - Z_{12} \right) z_l}{\cdots} = 0 \qquad (7)$$

From this result, it is shown that if $T_2 = Z_{12} + Z_{13}$, then full cancellation in the common-mode can be achieved. With the common-mode cancellation constraint met, the result is then inserted back into the original transfer function in (10) to find the constraint placed on the differential-mode compensation:

$$H(s) = \frac{Z_{13} \left(Z_{12} + Z_{23} + Z_{13} + Z_{22} \right)}{\cdots} = 0 \qquad (8)$$

The numerator of this result contains no terms of T_3 in which to tune in comparison to the terms of the impedance matrix. Additionally, the terms of the impedance matrix in a cylindrically or concentrically wound coil configuration are positive, preventing simple geometries from creating a zero in the transfer function. If differential-mode compensation is to be achieved, this result seems to provide no opportunity for the transfer function to become zero, save for the possibility of making $Z_{13} = 0$. In the case where Z_{13} can be made zero, the transfer function denominator would remain finite and non-zero, representing a possible condition to generate a

zero for the transfer function, if the structure can be arranged to provide it.

Another consideration may apply in this case. In past work [6] it was shown that depending on the frequency range of interest, filter performance, even with imperfect cancellation, may be perfectly adequate for practical purposes. With imperfect cancellation, a new term Δ_2 can be defined to be the effective residual shunt-path impedance of the capacitor. More specifically, $\Delta_2 = T_2 - (Z_{12} + Z_{13})$. If this is substituted into the general condition in (6), and with the resulting equation rearranged, (9) results. This provides a relation where Z_{13} is not explicitly required to be zero for the transfer function to become zero.

$$0 = Z_{13} \left(T_2 + Z_{22} + Z_{23} \right) - \Delta_2 \left(T_3 - Z_{23} \right) \qquad (9)$$

Hence, one may gain good performance in both common-mode and differential-mode by realizing substantial (but not perfect) cancellation in common-mode to benefit differential-mode performance.

D. Simulation and Model Validation

To validate the model and transfer function analysis, the common- and differential-mode filters constructed in Section II-C are used as the basis for simulation, excluding the coupling between the two coils. Each of the measurements presented in the section is simulated here using the model developed, to allow comparison to the experimental results.

To simulate both common- and differential-mode responses, the equivalent circuit models for each mode are constructed. These equivalent circuit models, shown in Fig. 20, include the inductance compensation windings, as well as the equivalent series resistance and equivalent series inductance of each capacitor. This allows for the direct use of (10) from Appendix I, the transfer function of the circuit in Fig. 19.
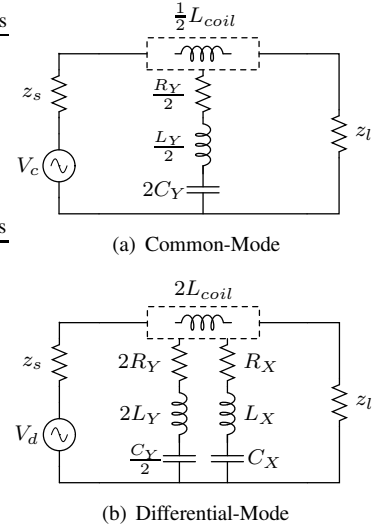
(a) Common-Mode

(b) Differential-Mode

Fig. 20. Common- and differential-mode equivalent circuits used to simulate the filters in Section II-C.

In the simulation, both the line-to-ground (Y) capacitor (Panasonic ECK-ATS472ME6) and the line-to-line (X) capac-

itor (Rubycon 250MMCA334KUV) are modeled with first-order equivalent series resistance, equivalent series inductance, and bulk capacitance. The nominal value of capacitance, along with the measured values of inductance and resistance, are used in the model of each capacitor. The Y capacitor parameters are R_Y=200mΩ, L_Y=48.6nH, C_Y=4700pF; the X capacitor parameters are R_X=50mΩ, L_X=49.4nH, C_X=330nF. The source (z_s) and load (z_l) impedances match those of the network analyzer, 50Ω. The coil used in the test filters, shown in Fig. 7, is represented by the inductance matrix L_{coil}, which is obtained using the numerical inductance calculation tool FastHenry:

$$L_{coil} = \begin{bmatrix} 36.52 & 42.62 & 0.236 \\ 42.62 & 224.6 & 8.089 \\ 0.236 & 8.089 & 5.262 \end{bmatrix} \text{nH}$$

For common-mode, T_3 is set to 1MΩ to approximate an open circuit, and T_2 is set to the effective impedance of the Y capacitor, $Z_{Y_{CM}} = \frac{1}{2}\left(R_Y + (j\omega C_Y)^{-1} + j\omega L_Y\right)$. For the differential-mode simulation, the effective impedance of the Y capacitor is different. With the two capacitors in series, the effective impedance, and thus T_2, now becomes $Z_{Y_{DM}} = 2\left(R_Y + (j\omega C_Y)^{-1} + j\omega L_Y\right)$. The effective impedance of the X capacitor is $Z_{X_{DM}} = R_X + (j\omega C_X)^{-1} + j\omega L_X$, the value used for T_3.

The results of the common- and differential-mode simulations are shown in Fig. 21. Comparing the simulation results to the experimental data in Fig. 12, the differential-mode results do match in an absolute sense. The *Optimal Y (DM)* simulation is roughly between the two measured coupling cases, which is understandable given coupling between the coils is not modeled. However, the addition of the X capacitor in the *Optimal Y, Uncancelled X (DM)* fails to match the same downward-shift in resonance to near 20MHz, which exists in both experimental measurements. The shift of this resonance is representative of an increase in effective inductance in the Y capacitor branch, which may be a result of unmodeled inductive coupling between the X and Y capacitors. The important similarity between the experimental measurements and the simulation is seen comparing *Optimal Y, Uncancelled X (DM)* and the final trace *Optimal Y, Optimal X (DM)*. By appropriately locating the X capacitor on the coil, it is possible to both shift the resonance higher in frequency, and to increase the attainable attenuation.

If consideration is given to modeling the increase in effective inductance in the Y capacitor branch when the X capacitor is present, significantly improved correlations between the experimental measurements and the model simulation result. If $Z_{Y_{DM}} = 2\left(R_Y + (j\omega C_Y)^{-1} + j\omega\left(L_Y + 0.2L_Y\right)\right)$, which represents a modest 20% increase in effective inductance, and slightly moving (by 1.5mm) the tuning location of the X capacitor on the coil to yield a refined inductance matrix,

$$L_{coil} = \begin{bmatrix} 36.52 & 42.29 & 0.563 \\ 42.29 & 222.4 & 9.091 \\ 0.563 & 9.091 & 5.432 \end{bmatrix} \text{nH}$$
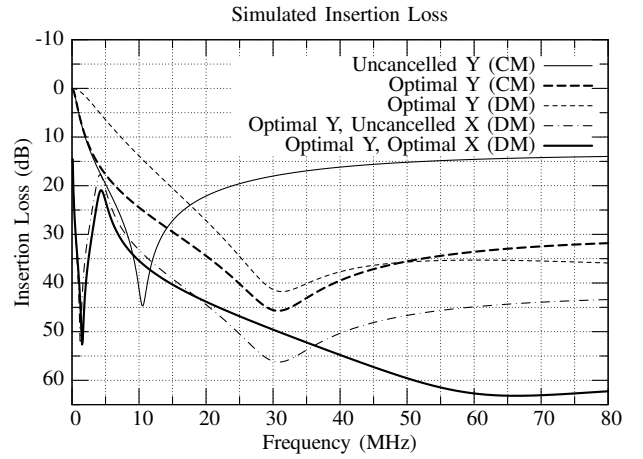

Fig. 21. Simulated results for the filters in Section II-C, using the circuits shown in Fig. 20. Note the different frequency range than in Fig. 12.

the plot in Fig 22 results. These results correlate significantly better than the case without the added effective inductance, although differences are still notable for *Optimal Y, Uncancelled X (DM)*.

Given the substantial modeling simplifications used in creating these simulations (e.g. neglecting coil-to-coil and other mutual couplings, using simple numerical simulations to obtain coil inductances, etc.) the degree of accuracy of the model is striking, confirming its usefulness for understanding the behavior of such systems.
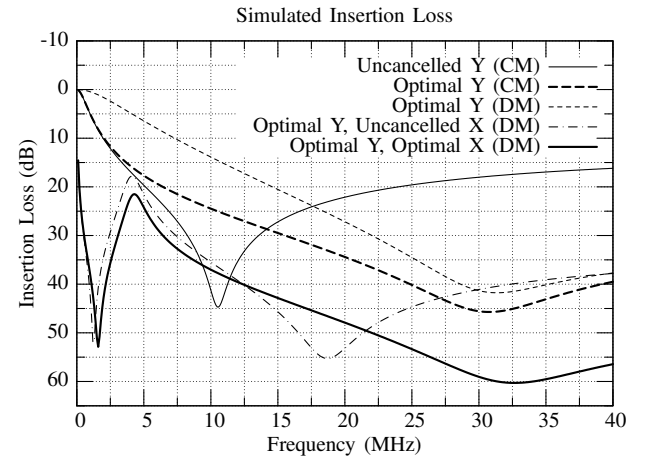

Fig. 22. Simulated results for the filters in Section II-C, using the circuits shown in Fig. 20 with additional differential-mode Y capacitor inductance.

V. CONCLUSION

The size and performance of EMI filters are often limited by their component parasitics, such as the equivalent series inductance of capacitors. Past work has shown that a coupled magnetic winding can be used to cancel the effects of a single capacitor's parasitic inductance, thereby substantially improving filter performance.

This paper has built on previous work by demonstrating the use of a single coupled magnetic winding to compensate for the effects of the parasitic inductances of two discrete capacitors. This work was applied experimentally to both test filters and to a commercially-available EMI filter with great success. Further, the coupling of closely oriented magnetic windings was also investigated, illustrating their successful use in constrained spaces, and a possible avenue for optimizing winding size. Finally, an analytical basis for the inductance compensation is developed and compared to experimental results.

APPENDIX I
THREE-PORT TAPPED-INDUCTOR EXTENDED CANTILEVER MODEL TRANSFER FUNCTION

Equation (10) gives the analytic solution of the transfer function from input voltage V_{in} to output voltage V_l for the circuit in Fig. 19. The result was found using direct circuit analysis, with the source network consisting of an input voltage source V_{in} with series impedance z_s, and a load network comprised of an impedance z_l. T_2 and T_3 are arbitrary impedances representing the two capacitors.

$$H(s) = \frac{\begin{aligned}(T_2 T_3 - Z_{13} T_3 - Z_{12} T_3 - Z_{23} T_2 \\ -Z_{13} T_2 + Z_{12} Z_{23} - Z_{13} Z_{22})\, z_l\end{aligned}}{\begin{aligned}&T_3 z_l z_s + T_2 z_l z_s + Z_{22} z_l z_s + T_2 T_3 z_s \\ &+ Z_{33} T_3 z_s + 2 Z_{23} T_3 z_s + Z_{22} T_3 z_s \\ &+ Z_{33} T_2 z_s + Z_{22} Z_{33} z_s - Z_{23}^2 z_s \\ &+ T_2 T_3 z_l + Z_{11} T_3 z_l + Z_{22} T_2 z_l + 2 Z_{12} T_2 z_l \\ &+ Z_{11} T_2 z_l + Z_{11} Z_{22} z_l - Z_{12}^2 z_l \\ &+ Z_{33} T_2 T_3 + 2 Z_{23} T_2 T_3 + Z_{22} T_2 T_3 \\ &+ 2 Z_{13} T_2 T_3 + 2 Z_{12} T_2 T_3 + Z_{11} T_2 T_3 \\ &+ Z_{11} Z_{33} T_3 + 2 Z_{11} Z_{23} T_3 + Z_{11} Z_{22} T_3 \\ &- Z_{13}^2 T_3 - 2 Z_{12} Z_{13} T_3 - Z_{12}^2 T_3 + \\ &Z_{22} Z_{33} T_2 + 2 Z_{12} Z_{33} T_2 + Z_{11} Z_{33} T_2 \\ &- Z_{23}^2 T_2 - 2 Z_{13} Z_{23} T_2 - Z_{13}^2 T_2 \\ &+ Z_{11} Z_{22} Z_{33} - Z_{12}^2 Z_{33} - Z_{11} Z_{23}^2 \\ &+ 2 Z_{12} Z_{13} Z_{23} - Z_{13}^2 Z_{22}\end{aligned}} \quad (10)$$

ACKNOWLEDGMENT

REFERENCES

[1] T. K. Phelps and W. S. Tate, "Optimizing passive input filter design," in *Proceedings of the Sixth National Solid-State Power Conversion Conference*, May 1979, pp. G1.1–G1.10.

[2] H. W. Ott, *Noise Reduction Techniques in Electronic Systems*, 2nd ed. John Wiley & Sons, 1988.

[3] C. Sullivan and A. Kern, "Capacitors with fast current switching require distributed models," in *Proceedings of the IEEE Power Electronics Specialists Conference*, vol. 3, Vancouver, BC, June 2001, pp. 1497–1503.

[4] Uchida, Katsuyuki, Sugitani, and Masami, "Lc filter with capacitor electrode plate not interfering with flux of two coils," U.S. Patent 6 476 689, November 5, 2002.

[5] T. Neugebauer, J. Phinney, and D. Perreault, "Filters and components with inductance cancellation," *IEEE Transactions on Industry Applications*, vol. 40, no. 2, pp. 483–491, March-April 2004.

[6] T. Neugebauer and D. Perreault, "Filters with inductance cancellation using printed circuit board transformers," *IEEE Transactions on Power Electronics*, vol. 19, no. 3, pp. 591–602, May 2004.

[7] D. Perreault, J. Phinney, and T. Neugebauer, "Filter having parasitic inductance cancellation," U.S. Patent 6 937 115, August 30, 2005.

[8] S. Wang, F. Lee, D. Chen, and W. Odendaal, "Effects of parasitic parameters on emi filter performance," *IEEE Transactions on Power Electronics*, vol. 19, no. 3, pp. 869–877, May 2004.

[9] S. Wang, F. Lee, and W. Odendaal, "Using a network method to reduce the parasitic parameters of capacitors," in *Proceedings of the IEEE Power Electronics Specialists Conference*, vol. 1, June 2004, pp. 304–308.

[10] S. Wang, F. Lee, W. Odendaal, and J. van Wyk, "Improvement of emi filter performance with parasitic coupling cancellation," *IEEE Transactions on Power Electronics*, vol. 20, no. 5, pp. 1221–1228, September 2005.

[11] T. Neugebauer and D. Perreault, "Parasitic capacitance cancellation in filter inductors," in *Proceedings of the IEEE Power Electronics Specialists Conference*, vol. 4, June 2004, pp. 3102–3107.

[12] R. Chen, J. van Wyk, S. Wang, and W. Odendaal, "Improving the characteristics of integrated emi filters by embedded conductive layers," *IEEE Transactions on Power Electronics*, vol. 20, no. 3, pp. 611–619, May 2005.

[13] A. Kamon, L. Silveira, C. Smithhisler, and J. White, *FastHenry USER'S GUIDE*, 3rd ed., MIT Research Laboratory of Electronics, Cambridge, MA 02139 U.S.A., November 1996.

[14] *CORCOM Product Guide Catalog 1654001*, Tyco Electronics, Libertyville, Illinois 60048 U.S.A, March 2004.

[15] D. Maksimovic, R. Erickson, and C. Griesbach, "Modeling of cross-regulation in converters containing coupled inductors," *IEEE Transactions on Power Electronics*, vol. 15, no. 4, pp. 607–615, July 2000.

[16] K. Changtong, R. Erickson, and D. Maksimovic, "A comparison of the ladder and full-order magnetic models," in *Proceedings of the IEEE Power Electronics Specialists Conference*, vol. 4, Vancouver, BC, June 2001, pp. 2067–2071.

[17] J. Hayes, N. O'Donovan, and M. Egan, "The extended t model of the multiwinding transformer," in *Proceedings of the IEEE Power Electronics Specialists Conference*, vol. 3, June 2004, pp. 1812–1817.

[18] K. Ngo, S. Srinivas, and P. Nakmahachalasint, "Broadband extended cantilever model for magnetic component windings," *IEEE Transactions on Power Electronics*, vol. 16, no. 4, pp. 551–557, July 2001.

[19] K. Ngo and A. Gangupomu, "Improved method to extract the short-circuit parameters of the becm," *IEEE Power Electronics Letters*, vol. 1, no. 1, pp. 17–18, 2003.